Title
Spire stimulates nucleation by Cappuccino and binds both ends of actin filaments

Journal
Molecular Biology of the Cell, 31(4)

ISSN
1059-1524

Authors
Bradley, Alexander O
Vizcarra, Christina L
Bailey, Hannah M
et al.

Publication Date
2020-02-15

DOI
10.1091/mbc.e19-09-0550

Peer reviewed

Spire stimulates nucleation by Cappuccino and binds both ends of actin filaments

Alexander O. Bradley[a], Christina L. Vizcarra[a,†], Hannah M. Bailey[a], and Margot E. Quinlan[a,b,*]
[a]Department of Chemistry and Biochemistry and [b]Molecular Biology Institute, University of California, Los Angeles, Los Angeles, CA 90095

ABSTRACT **The actin nucleators Spire and Cappuccino synergize to promote actin assembly, but the mechanism of their synergy is controversial. Together these proteins promote the formation of actin meshes, which are conserved structures that regulate the establishment of oocyte polarity. Direct interaction between Spire and Cappuccino is required for oogenesis and for in vitro synergistic actin assembly. This synergy is proposed to be driven by elongation and the formation of a ternary complex at filament barbed ends, or by nucleation and interaction at filament pointed ends. To mimic the geometry of Spire and Cappuccino in vivo, we immobilized Spire on beads and added Cappuccino and actin. Barbed ends, protected by Cappuccino, grow away from the beads while pointed ends are retained, as expected for nucleation-driven synergy. We found that Spire is sufficient to bind barbed ends and retain pointed ends of actin filaments near beads and we identified Spire's barbed-end binding domain. Loss of barbed-end binding increases nucleation by Spire and synergy with Cappuccino in bulk pyrene assays and on beads. Importantly, genetic rescue by the loss-of-function mutant indicates that barbed-end binding is not necessary for oogenesis. Thus, increased nucleation is a critical element of synergy both in vitro and in vivo.**

Monitoring Editor
Laurent Blanchoin
CEA Grenoble

Received: Sep 30, 2019
Revised: Dec 5, 2019
Accepted: Dec 18, 2019

INTRODUCTION

Cells contain varied actin-based structures that fulfill distinct functional roles. The actin cytoskeleton is malleable due to dynamic structural regulation by a range of distinct actin-binding proteins. The first step to building a structure is generally catalysis of new actin filaments, so-called nucleation. Both a kinetic barrier and certain actin-binding proteins, such as profilin, prevent spontaneous nucleation in the cell. Instead, actin nucleators stimulate this process in highly regulated manners. There are three known classes of actin nucleators that function by distinct mechanisms: the Arp2/3 complex, formins, and tandem-WH2 domain nucleators. A developing trend is that none of these proteins works independently. Effector proteins can inhibit or enhance the activity of actin nucleators. Usually, the effector is not a nucleator. In some cases, two independent nucleators also work together. A poorly understood example of such interplay is the collaboration between Cappuccino (Capu, a formin) and Spire (Spir, a tandem-WH2 nucleator).

Both Spir and Capu are required for oogenesis. This discovery was first made in *Drosophila* and subsequently demonstrated in mice (Manseau and Schupbach, 1989; Leader *et al.*, 2002; Pfender *et al.*, 2011). In both cases, Capu (or Fmn-2, one of two mammalian homologues) and Spir (or mSpire, referring to mammalian homologues, Spire-1 and Spire-2) build a mesh of actin that fills the oocyte (Dahlgaard *et al.*, 2007; Azoury *et al.*, 2008; Schuh and Ellenberg, 2008; Pfender *et al.*, 2011). The discovery that both Spir and Capu are actin nucleators led to the question of why two nucleators would be needed to build one structure (Quinlan *et al.*, 2005). We now know that direct interaction between Spir and Capu is required for their function (Quinlan, 2013). Detailed biochemical analyses and structural biology provide insight into the interaction:

This article was published online ahead of print in MBoC in Press (http://www.molbiolcell.org/cgi/doi/10.1091/mbc.E19-09-0550) on December 26, 2019.

The authors declare no competing financial interests.

Author contributions: M.E.Q. (lead) and C.L.V. (supporting) conceptualized the experiments. A.O.B. (lead) and C.L.V. (supporting) developed the methodology. A.O.B. performed and analyzed all experiments; with the exception of genetics experiments presented in Table 1 and Figure 7, performed by H.M.B., and seeded elongation experiments presented in Figure 5, A and B, performed by C.L.V. A.O.B. prepared all figures. M.E.Q. and A.O.B. wrote the manuscript. All authors contributed to discussion and evaluation of the manuscript.

†Present address: Department of Chemistry, Barnard College, 3009 Broadway, New York, NY 10027.

*Address correspondence to: Margot E. Quinlan (margot@chem.ucla.edu).

Abbreviations used: GFP, green fluorescent protein; KIND, kinase noncatalytic C-lobe domain; NPF, nucleation promoting factor; OG, Oregon Green; TIRF, total internal reflection fluorescence; WH2, Wasp homology 2.

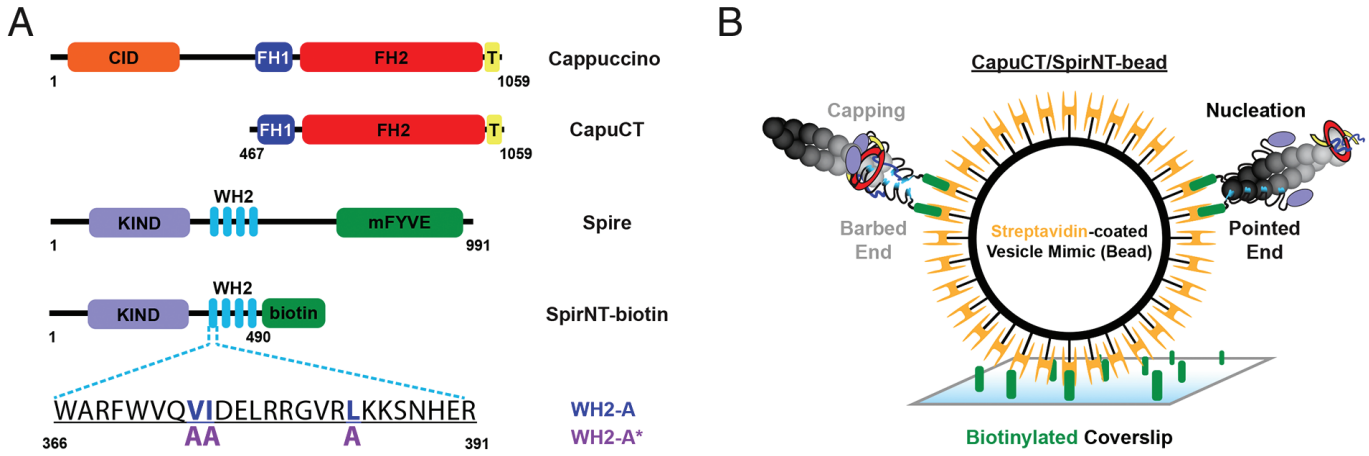

FIGURE 1: Domain architecture and bead methodology. (A) Domain architecture of *Drosophila melanogaster* Cappuccino (Capu), Spire (Spir), and truncations used. CID, Capu inhibitory domain (orange); FH1/FH2, formin homology domains (1, dark blue; 2, red); T, tail (yellow); KIND, kinase noncatalytic C-lobe domain (purple); WH2, Wiskott-Aldrich syndrome homology domains (light blue); mFYVE, modified FYVE (zinc finger) domain (green). Spir has four WH2 domains, named WH2-A through WH2-D. The sequence of WH2-A and mutations that disrupt its actin binding are shown. (B) Bead experiment methodology. To decorate streptavidin-coated microspheres (gold) with SpirNT, and to bind the microspheres to the coverslip, biotin (green) is conjugated both to coverslips and to SpirNT. Two potential orientations of the actin filament distinguish Spir's primary activities at each end: capping filaments at their barbed ends (left) and nucleating filaments from their pointed ends (right).

the N-terminal Spir-KIND domain binds the C-terminal Capu-tail with ~100 nM affinity (Figure 1; Quinlan *et al.*, 2007; Pechlivanis *et al.*, 2009; Vizcarra *et al.*, 2011; Zeth *et al.*, 2011). However, our understanding of the functional consequences of the interaction remains incomplete. Capu, like all formins, is a dimer. It can bind two copies of Spir and, thereby, accelerate actin assembly by Spir (Quinlan *et al.*, 2007; Vizcarra *et al.*, 2011). In contrast, Spir's KIND domain inhibits nucleation by Capu and competes with barbed ends for Capu binding, effectively inhibiting Capu's ability to accelerate actin assembly (Quinlan *et al.*, 2007; Vizcarra *et al.*, 2011). However, when a human Spire-1 construct, containing both the KIND domain and four tandem WH2 domains, is mixed with the C-terminal half of Fmn-2, actin assembly is greatly enhanced (Montaville *et al.*, 2014). So-called ping-ponging—Spir and Fmn-2 alternately binding to the barbed end of filaments—is observed and was proposed to account for synergistic actin assembly (Montaville *et al.*, 2014).

Spir is enriched at the cortex of the *Drosophila* oocyte and localizes to Rab11-positive vesicles in mouse oocytes, and the C-terminal mFYVE domain of mSpire-1 binds phospholipids (Quinlan *et al.*, 2007; Pfender *et al.*, 2011; Quinlan, 2013; Tittel *et al.*, 2015). While Fmn-2 is also observed on Rab11-positive vesicles in mouse oocytes, GFP-Capu appears diffuse throughout the *Drosophila* oocyte (Dahlgaard *et al.*, 2007; Schuh, 2011; Quinlan, 2013). In the mouse oocyte, Rab11-positive vesicles that contain mSpire, Fmn-2, and myosin V are at nodes of the actin mesh that fills the oocyte (Schuh, 2011). Mesh dynamics contribute to nucleus positioning and long distance transport of the Rab11-positive vesicles toward the cell cortex (Holubcová *et al.*, 2013; Almonacid *et al.*, 2015; Ahmed *et al.*, 2018). A model to account for the long distance transport includes mSpire/Fmn-2–nucleated actin filaments growing with their barbed ends remaining near the vesicles, creating tracks that myosin V on neighboring vesicles can walk along, pulling vesicles together (Schuh, 2011). When ping-ponging was observed in vitro, Montaville *et al.* (2014) expanded on this model, proposing that barbed ends of filaments and/or prenuclei are recruited by vesicle-bound mSpire and handed off to Fmn-2 to stimulate elongation.

To learn more about how Spir and Capu interact to build actin filaments and structures, we combined biochemistry and fly genetics. We developed a bead-based assay, in which we attached the N-terminal half of Spir (SpirNT) to beads and added the unconjugated C-terminal half of Capu (CapuCT), based on reported localization data (see Figure 1A for construct definitions). Through this work we found that beads decorated with SpirNT and CapuCT (CapuCT/SpirNT-beads) nucleate filaments that grow with their barbed ends away from beads, protected by CapuCT, opposite to the polarity expected based on the ping-pong model. We found that SpirNT alone on beads (SpirNT-beads) nucleates filaments oriented the same way. We also found that SpirNT-beads retain the pointed ends of filaments at the bead with a dwell time of ~100 s while neighboring SpirNT-beads capture and cap the barbed ends of filaments for several hundreds of seconds. Next, we identified the domain necessary for Spir's high-affinity barbed-end binding. Surprisingly, barbed-end binding is not necessary for oogenesis and loss of barbed-end binding increases Spir/Capu synergy in vitro. These genetic and biochemical data indicate that ping-ponging at the barbed end is neither the dominant source of synergy nor necessary in vivo. Instead, enhanced nucleation by the Spir/Capu complex is critical.

RESULTS

Barbed ends project away from CapuCT/SpirNT-beads

To learn more about how Spir and Capu interact to build actin filaments and structures, we developed a bead-based assay. Spir is enriched at the cortex of the *Drosophila* oocyte, localizes to Rab11-positive vesicles in mouse oocytes, and the C-terminal mSpire-mFYVE domain binds phospholipids (Quinlan *et al.*, 2007; Quinlan, 2013; Pfender *et al.*, 2011; Tittel *et al.*, 2015). While Fmn2 is also observed on vesicles in the mouse oocyte, GFP-Capu appears diffuse throughout the *Drosophila* oocyte (Schuh, 2011; Quinlan, 2013). On the basis of these data, we immobilized SpirNT on beads and added unconjugated CapuCT. To do so, we biotinylated a C-terminal Avitag on SpirNT and mixed it with CapuCT. We then attached these complexes to streptavidin-coated beads under

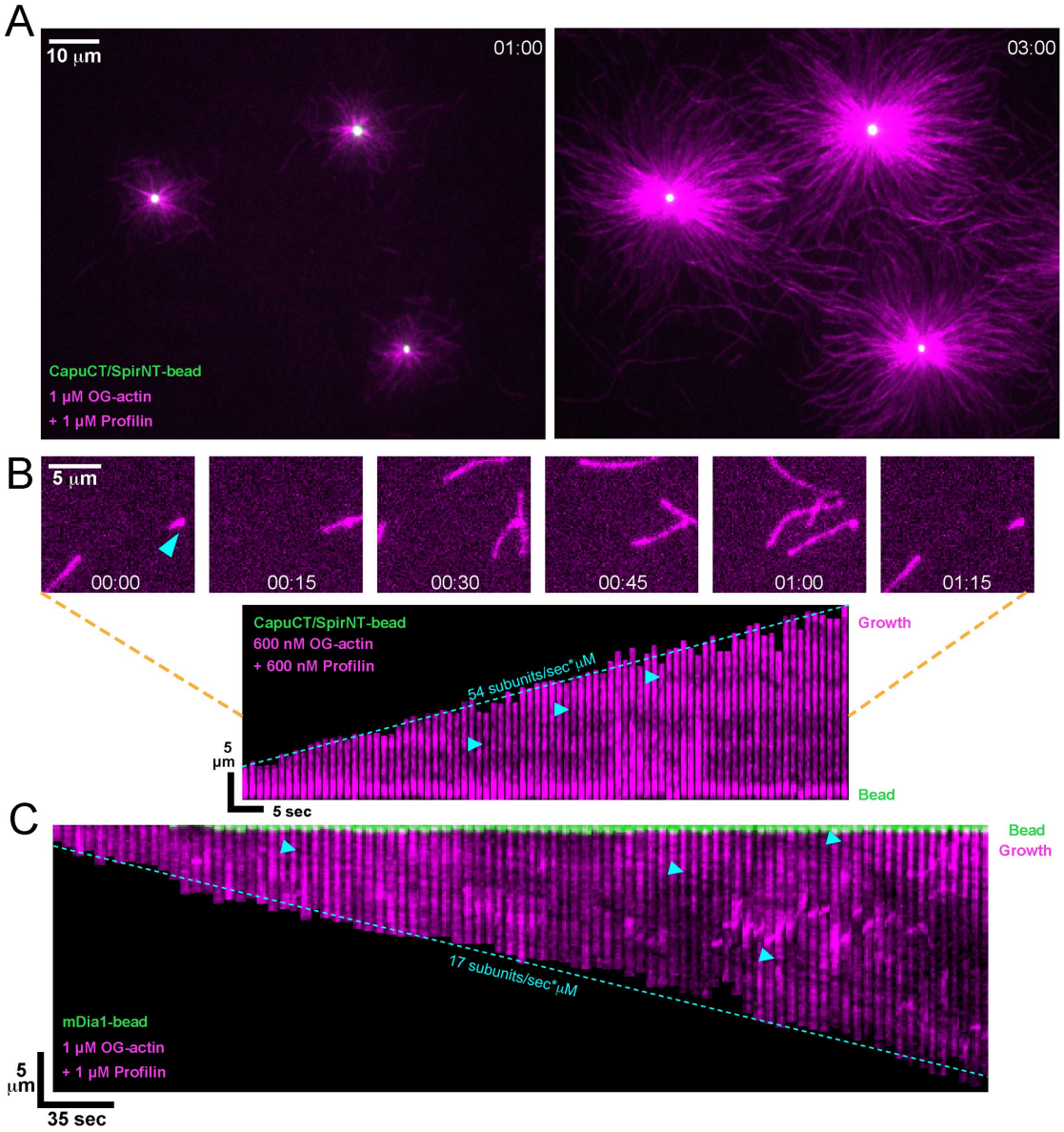

FIGURE 2: Barbed ends project away from CapuCT/SpirNT-beads. (A) Actin assembles off of CapuCT/SpirNT-beads. See also Supplemental Video 1. (B) A single filament is nucleated and retained by a bead. Kymograph (bottom) shows fiducial marks, such as bleached filament regions, which do not move with respect to the bead (cyan triangles). New, labeled actin is added away from the bead, indicating growth away from the bead. See Supplemental Video 2 for another example of retention by CapuCT/SpirNT-beads. (C) A single filament is nucleated and elongated by a bead coated with mDia1. Fiducial marks (highlighted with cyan triangles) in the kymograph are displaced from the bead at the rate of elongation, indicating growth at the bead. See also Supplemental Video 3.

saturating conditions (Figure 1B). We introduced the decorated beads to a sparsely biotinylated flow chamber to visualize them with total internal reflection fluorescence (TIRF) microscopy. Any unbound SpirNT or CapuCT was washed away. When we added actin (20% OG-actin) and profilin to the flow chamber, extensive and rapid polymerization followed (Figure 2A and Supplemental Video 1).

Two groups proposed that Spir/Capu-coated vesicles have filaments with barbed ends apposed to the vesicle and pointed ends growing away (Figure 1B; Schuh, 2011; Montaville *et al.*, 2014). We tested this model by examining the orientation of filaments growing off of CapuCT/SpirNT-beads. By lowering the concentration of actin (600 nM), we decreased nucleation such that we could track individual filaments. Under these conditions, we observed filaments growing from but "retained" at the beads (Supplemental Video 2). We carefully analyzed nine individual filaments. In every case, fiducial marks that do not move with respect to the bead, and increased fluorescence intensity at filament ends (i.e., ends brighter due to the addition of unbleached monomers [Kovar and Pollard, 2004]), away from the bead, indicated that barbed ends grow away from the bead surface (Figure 2B). Filaments growing under these conditions elongated away from the bead at a rate of 50 ± 16 s^{-1} μM^{-1} (mean ± SD, n = 11), consistent with Capu-mediated elongation. We expected to see the opposite orientation of filaments with Capu directly conjugated to the beads. For unknown reasons, Capu was not functional when attached to beads through a number of different linkers. Instead, we conjugated the formin mDia1 to beads. In this case, fiducial marks were displaced at the rate of filament elongation (~17 s^{-1} μM^{-1}) and the addition of

unbleached monomers was no longer observed at the filament end away from the bead (Figure 2C and Supplemental Video 3), consistent with barbed-end growth at the bead surface. Together these data demonstrate that CapuCT/SpirNT-beads nucleate filaments with barbed ends growing away from the bead and suggest that CapuCT separates from SpirNT to elongate the filament.

Spir-beads retain the pointed ends of nucleated actin filaments

A dense collection of filaments emanated radially from CapuCT/SpirNT-beads. Because we concluded that CapuCT-mediated elongation proceeded away from the beads, the density of actin near the bead surface suggested that the pointed ends of filaments could be retained by Spir. We repeated the experiments with SpirNT-beads, without added CapuCT or profilin, and observed similar patterns (Figure 3A and Supplemental Video 4). We found that nucleation by SpirNT-beads was suppressed enough to observe individual filaments by adding profilin (Figure 3B). We again observed filaments retained at and growing away from the bead surface (Figure 3C and Supplemental Video 5). Filaments growing away from SpirNT-beads elongated at a rate of 16.0 ± 0.3 s^{-1} μM^{-1} (mean ± SD, n = 12), as expected for free barbed ends. The filaments near the beads were released over time, demonstrating that they were not attached to the surface. The distribution of filament dwell times was well fit by a single exponential with an off rate of 0.007 ± 0.003 s^{-1} (n = 70; Figure 3D). We note that retention

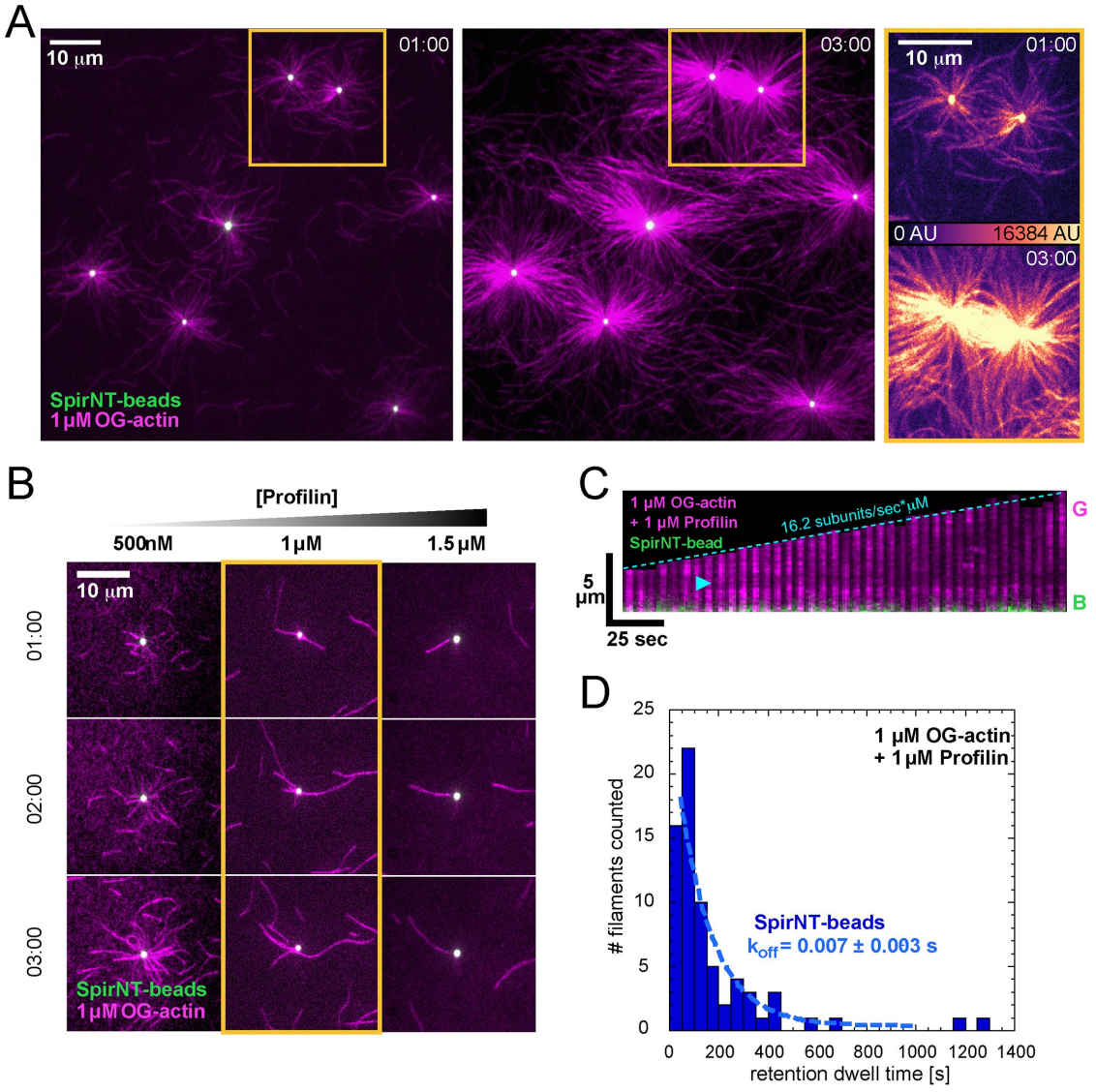

FIGURE 3: SpirNT-beads retain the pointed ends of nucleated actin filaments. (A) SpirNT-beads, in the absence of Capu and profilin, also potently polymerize actin. The highlighted region (gold) is magnified and pseudocolored (right) to emphasize the enrichment of actin filaments between beads. See also Supplemental Video 4. (B) Nucleation by SpirNT-beads is suppressed by profilin. When added at 1 μM (gold box), profilin permits the observation of several, individual filaments per bead. (C) SpirNT-beads also retain nucleated filaments. G, growth; B, bead. Fiducial marks (e.g., cyan triangle) in the kymograph are not displaced as the filament elongates, indicating growth away from the bead. See also Supplemental Video 5. (D) Dwell times of filament pointed ends on beads. Nucleated and retained filaments were tracked from SpirNT-beads in the presence of 1 μM actin and 1 μM profilin. All bead-associated filaments were counted unless obviously captured from solution or >1 μm in length when first visible. The data are well fit by a single exponential (k_{off} = 0.007 ± 0.003 s^{-1}, n = 70 filaments; four independent experiments).

of filaments by SpirNT-beads was independent of profilin (Supplemental Figure S1G and Supplemental Video 6). Furthermore, neither filament end was observed to interact with beads coated with Spir-KIND and CapuCT (Supplemental Figure S1F), indicating that retention is specifically mediated by Spir-WH2 domains.

We did not assume that filaments were oriented with their barbed ends out when nucleated by SpirNT-beads because Spir has been reported to bind both the barbed and pointed ends of filaments (Quinlan *et al.*, 2005; Bosch *et al.*, 2007; Ito *et al.*, 2011). mSpire1 caps barbed ends with high affinity and SpirNT binds pointed ends weakly (nM vs μM K_d's; Quinlan *et al.*, 2005; Bosch *et al.*, 2007; Montaville *et al.*, 2014). We closely analyzed 10 of the 70 filaments included in the retention data set. All 10 filaments, growing from SpirNT-beads, displayed fiducial marks that did not move with respect to the bead and typically had brighter filament ends away from the beads, consistent with barbed ends being oriented away from the beads (Figure 3C). Thus, we conclude that barbed ends grow away from SpirNT-beads and that SpirNT is sufficient to retain the pointed ends of actin filaments near beads for >100 s.

SpirNT-beads capture and cap the barbed ends of actin filaments

When we examined the dense actin networks emanating from beads, we also observed apparent connections between neighboring beads (Figure 3A). This pattern suggested to us that the barbed ends of actin filaments could also be associated with beads. Under conditions where individual filaments could be tracked, we observed the "capture" of filaments (Figure 4). The association of captured filaments with Spir-beads often outlasted the single-filament imaging window (10+ min), precluding measurement of an off rate and suggesting that the interaction is distinct from retention.

In addition to seeing filaments spanning two beads, we often observed capture of free filaments. We probed the orientation of captured filaments using two colors of actin. We initiated elongation in the presence of Cy3B-actin and stabilized these filaments with phalloidin after several minutes. Adding a limiting pool of OG-actin (600 nM) plus profilin to favor barbed-end growth, we observed that, whether the filament had both ends free (as shown) or one end retained by a bead, only the barbed ends of filaments were captured by beads (Figure 4A and Supplemental Video 7). Filaments captured by beads did not grow measurably, suggesting that they are capped at their barbed ends (Figure 4A). Consistent with this conclusion, the fluorescence intensity of the filament near the bead steadily declined after binding (Figure 4B). Occasionally, we observed the release of a barbed end, following capture. In these cases, the filament resumed elongation at the same rate as before capture (Figure 4A). As noted above, barbed ends do not interact with CapuCT/Spir-KIND-beads (Supplemental Figure S1F). These data indicate that the barbed ends are capped by Spir-WH2 domains, as opposed to being nonspecifically stuck to the beads or KIND domain.

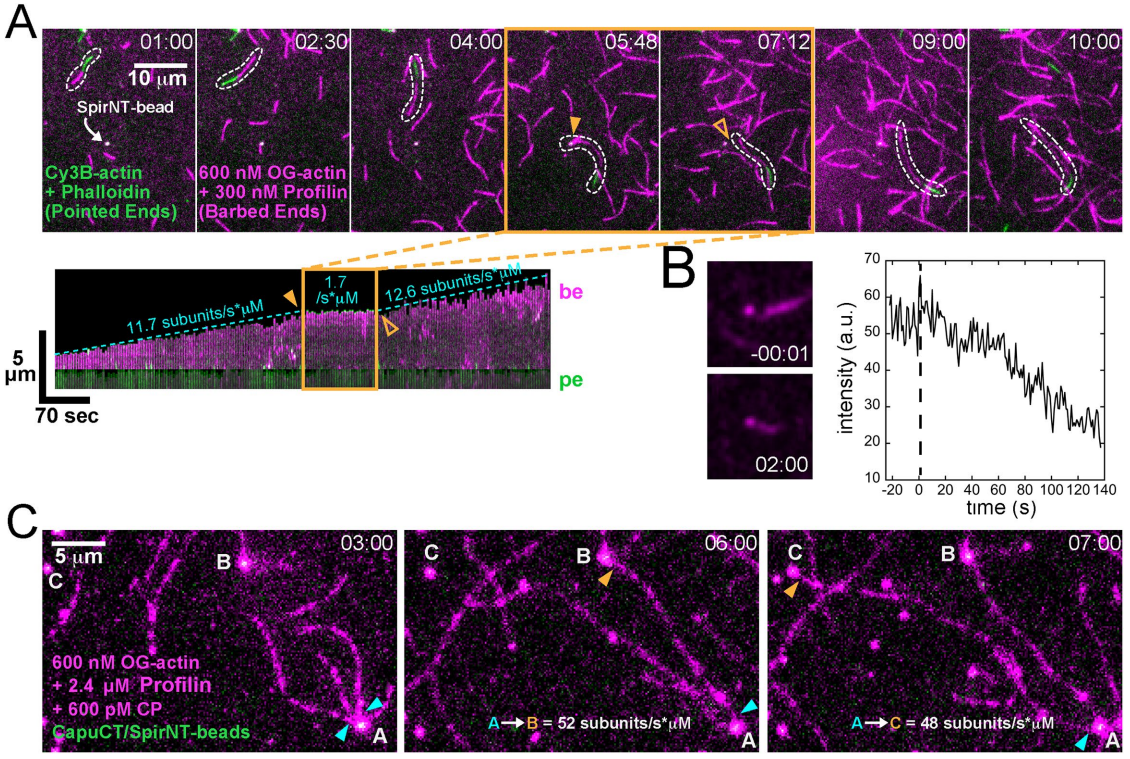

FIGURE 4: SpirNT-beads capture and cap the barbed ends of actin filaments. (A) Nucleated filaments (green) grow only at their barbed ends (magenta). A free filament (dashed outline) diffuses and grows until it is captured by a SpirNT-bead (solid triangle). The filament resumes growth once released by the bead (open triangle). The kymograph shows that the growing, barbed end (magenta) is captured/capped by Spir and resumes growth after release. See also Supplemental Video 7. (B) Intensity of filament ends decrease after bead capture. Images of a filament immediately before attachment and 2 min later. The intensity of the first 1 μm of this filament is plotted vs. time, with 0 s set to the capture event. (C) Two filaments (cyan triangles) nucleated by a SpirNT/CapuCT-bead (A) are retained for more than 5 min. Their barbed ends are captured (gold triangles) by other CapuCT/SpirNT-beads (B and C). Accelerated growth of these filaments (~50 subunits/s*μM) in the presence of profilin and capping protein indicates that CapuCT is elongating and protecting their barbed ends. Filaments did not measurably grow, following capture, suggesting that CapuCT is displaced and that the barbed end is bound by SpirNT upon capture. See also Supplemental Video 8.

To further study the phenomenon of filament capture, we added capping protein and CapuCT to the experiment. Under these conditions we observed sustained and accelerated growth (51 ± 11 s^{-1} μM^{-1}, mean ± SD, $n = 3$) of retained filaments or absence of growth ($n = 2$), confirming that CapuCT can separate from SpirNT and protect growing filament barbed ends from capping protein (Figure 4C). Growing filaments were still captured by beads, suggesting that SpirNT displaces CapuCT from the barbed end (Figure 4C and Supplemental Video 8). Together these data demonstrate that, with or without CapuCT present, Spir-beads can nucleate and retain the pointed ends of actin filaments, while neighboring beads can capture and cap their barbed ends.

Spir's WH2-A binds filament barbed ends and reduces actin nucleation

Each of Spir's four WH2 domains contributes differently to nucleation and they bind actin monomers with a range of affinities (from ~100 nM to 1.1 μM; Quinlan *et al.*, 2005; Rasson *et al.*, 2015). We reasoned that the N-terminal-most WH2 domain, WH2-A, binds barbed ends of filaments, based on our earlier observation that isolated WH2-A is the only Spir-WH2 domain that slows filament growth (Rasson *et al.*, 2015). To test the contribution of WH2-A to barbed-end binding, we first established that wild-type SpirNT caps barbed ends in a seeded elongation assay, as has been shown for mSpire-1 (Bosch *et al.*, 2007). In the presence of actin seeds, monomers, and profilin, SpirNT potently inhibited elongation (Figure 5A). The dose dependence of inhibition indicates an apparent affinity of SpirNT for barbed ends of 20 ± 3 nM, similar to that reported for mSpire-1 (Figure 5B). We then mutated three conserved, hydrophobic residues in WH2-A of SpirNT (SpirNT(A*); Figure 1A) to remove actin monomer binding by this domain alone. These mutations were previously shown to dramatically decrease, if not abolish, actin monomer binding (Quinlan *et al.*, 2005). When added to the seeded elongation assay, SpirNT(A*) was essentially unable to inhibit elongation (Figure 5, A and B). Thus, a functional WH2-A domain is necessary for high-affinity, barbed-end capping.

In standard pyrene-actin assays, we found that SpirNT(A*) assembled actin more potently than wild-type SpirNT (Figure 5C and Supplemental Figure S1C). The plateau was consistently lower for wild type, suggesting that barbed-end binding by SpirNT is sufficient to change the critical concentration under these conditions. We also noted that the plateau of SpirNT(A*) pyrene traces did not decrease at high concentrations as is seen for wild-type SpirNT, suggesting that this mutant does not potently sequester actin monomers (Figure 5C; Quinlan *et al.*, 2005). We next attached biotinylated SpirNT(A*) to beads and added actin and profilin. Consistent with increased activity in pyrene assays, we observed faster accumulation of filaments from SpirNT(A*)-beads compared with wild-type SpirNT-beads (Figure 5D and Supplemental Video 9). To compare nucleation rates on beads, we measured the integrated intensity of actin within a band 1.6 μm away from the beads. At this proximity, we are minimally sensitive to filament elongation and interpret the intensity as proportional to the number of filaments; that is, nucleation. We measured time courses and calculated the rates of increase in OG-actin signal. The difference in rates indicates that nucleation by SpirNT(A*) is approximately three times stronger than wild-type SpirNT in the presence of profilin (Figure 6, D and E). We also measured the dwell times of filaments retained by SpirNT(A*)-beads. The off rate was not significantly different than that of wild type ($k_{off(WT)}$ = 0.007 ± 0.003 s^{-1}, $k_{off(A*)}$ = 0.011 ± 0.003 s^{-1}, Student's *t* test, $p = 0.98$; Figure 5E), indicating that WH2-A does not play an important role in filament retention. Notably, we rarely observed capture events by SpirNT(A*)-beads. In several cases, filaments appeared to be close enough to a neighboring bead for capture for tens of seconds, but sustained association of the barbed end with beads was rare. Taken together, these data are consistent with the requirement of functional WH2-A for high-affinity barbed-end binding and demonstrate that this domain is not critical for pointed-end binding.

Synergy between Spir and Capu does not require barbed-end binding

Previously, synergistic actin assembly by mSpire-1 and Fmn-2 was described: the rate of actin assembly by mSpire-1 + Fmn-2 is greater than the sum of assembly rates of the individual nucleators (Montaville *et al.*, 2014). We confirmed that SpirNT and CapuCT exhibit a similar synergistic effect in pyrene-actin assembly assays (Figure 6A and Supplemental Figure S1D). In the presence of profilin, the assembly rate of SpirNT + CapuCT (based on the $t_{1/2}$ at ≥40 nM SpirNT) was 6× and 15× faster than CapuCT or SpirNT, respectively (Figure 6B). As seen for the mammalian paralogues, direct interaction was required for synergy: SpirNT(Y232K), a mutant that does not bind Capu, does not synergize with CapuCT (Supplemental Figure S1E; Vizcarra *et al.*, 2011; Montaville *et al.*, 2014).

Montaville *et al.* (2014) concluded that actin assembly was enhanced by mSpire-1 and Fmn-2 alternately binding the barbed end, which they dubbed the ping-pong mechanism. Given that SpirNT(A*) does not bind to or capture barbed ends, we assume that ping-ponging is not possible with this mutant. However, when we tested SpirNT(A*) in the pyrene synergy assay, we found approximately three times enhanced synergy (based on the $t_{1/2}$ at ≥40 nM SpirNT), as opposed to loss of activity (Figure 6, A and B, and Supplemental Figure S1D). The dose dependence of synergy is indistinguishable for SpirNT and SpirNT(A*) (Figure 6B). We speculate that dose dependence is a function of Spir-KIND/Capu-tail binding, which should not be affected in SpirNT(A*). These data lead us to propose that enhanced nucleation, not just elongation, drives synergy when SpirNT and CapuCT interact.

To directly test whether nucleation is increased by SpirNT and CapuCT collaborating, we returned to the bead assay. When CapuCT/SpirNT-beads were mixed with actin and profilin, we observed potent nucleation (Figure 6C). Consistent with nucleation being a significant element of Spir/Capu synergy, the rate of filament formation was 6.5× greater than in the absence of Capu (Figure 6, C–E). Nucleation of profilin–actin by CapuCT/SpirNT(A*)-beads was even stronger than wild type (4×) and the synergy more pronounced (9.5× vs. SpirNT(A*)-beads in the absence of Capu) with the actin signal saturating at the measured 1.6 μm radius within ~2 min (Figure 6, C and D). Thus, nucleation is potently enhanced when SpirNT and CapuCT are combined and loss of barbed-end binding by SpirNT leads to even stronger nucleation in the presence and absence of CapuCT. These data indicate that enhanced nucleation is a major source of synergy in vitro.

Barbed-end binding is not necessary for oogenesis

Finally, we asked whether barbed-end binding is necessary for *Drosophila* oogenesis. To do so, we used full-length Spir (CG10076, splice variant "PB") with a C-terminal monomeric enhanced green fluorescent protein (GFP) tag in a genetic rescue assay. We mutated three conserved residues of WH2-A as done in vitro. We previously demonstrated that expression of wild-type Spir-GFP, driven by germline-specific nanos-Gal4-vp16, is sufficient to rescue fertility in flies that lack endogenous Spir (Table 1; Quinlan, 2013). We found

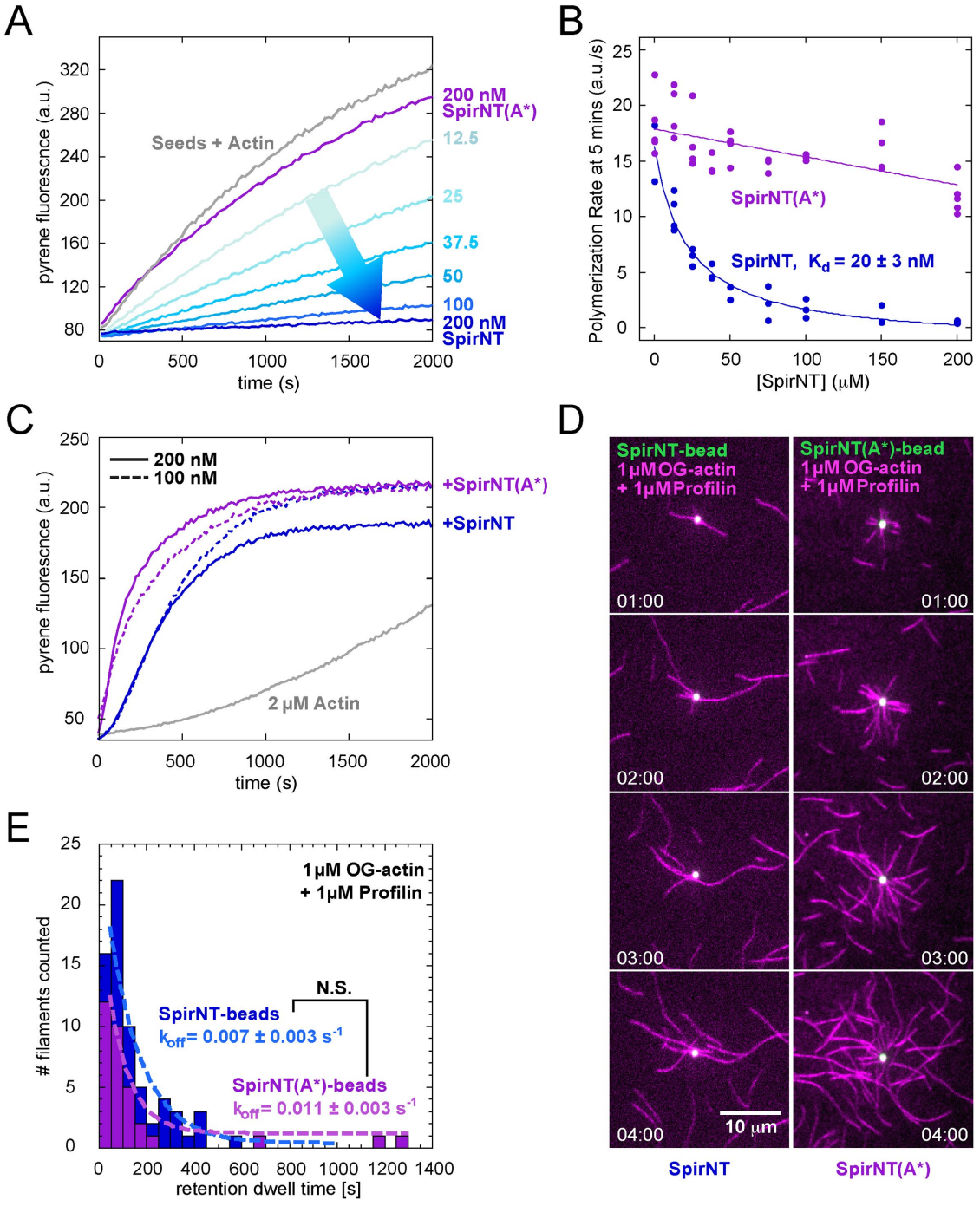

FIGURE 5: Spir's WH2-A binds filament barbed ends and reduces actin nucleation. (A) Seeded elongation is inhibited by the addition of 12.5–200 nM SpirNT (shades of blue). The addition of 200 nM SpirNT(A*) has no effect (purple). (B) Dose-dependent elongation rates are plotted for three experiments. The data are fit with a quadratic equation, indicating that SpirNT binds the barbed end with a K_d of 20 ± 3 nM. The line is a fit to all data points, and the K_d is the average of three independent experiments. Inhibition by SpirNT(A*) is negligible. (C) SpirNT(A*) assembles actin more potently than wild-type SpirNT in a pyrene–actin assembly assay. Plateaus that are independent of Spire concentration suggest that SpirNT(A*) does not sequester actin like SpirNT (compare solid lines). (D) SpirNT(A*)-beads nucleate more potently than wild type. See also Supplemental Video 9. (E) Quantification of filament pointed-end dwell times on beads (k_{off} = 0.011 ± 0.003 s^{-1}, n = 33 filaments; three independent experiments). The off rate is not significantly different from wild type (data from Figure 3D).

that fertility was largely rescued when Spir(A*)-GFP was expressed (hatch rate 40% compared with 59% for wild type; Table 1). Consistently, the mesh was present in 11 of 20 oocytes and streaming was properly regulated in about half of the oocytes observed (Figure 7, D and D'). Thus, barbed-end binding is not necessary for mesh formation or oogenesis, though the fertility decrease, relative to wild-type rescue, suggests that it may contribute under normal conditions.

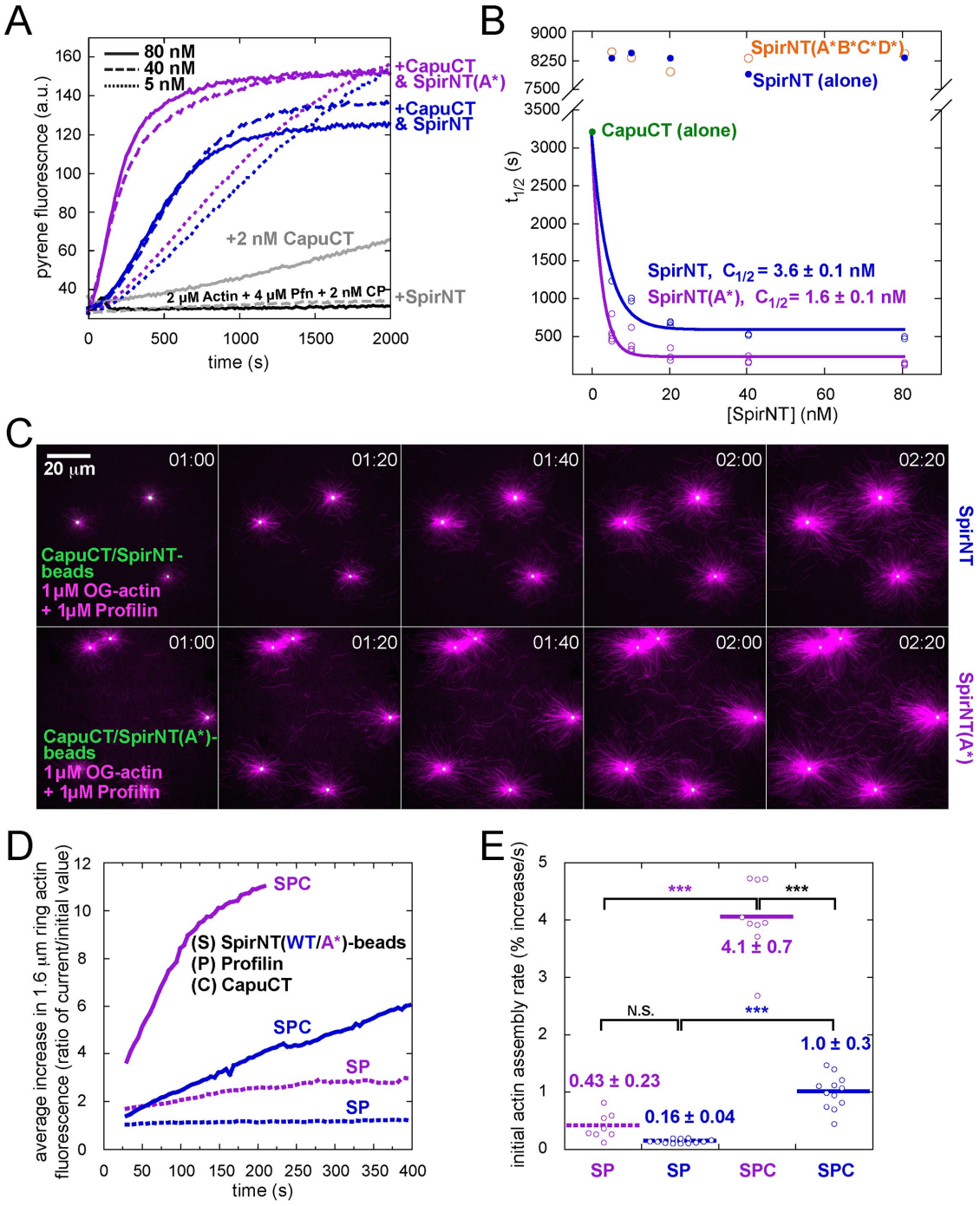

FIGURE 6: Synergy between Spir and Capu does not require barbed-end binding. (A) Actin assembly assays in the presence of profilin and capping protein. CapuCT alone and SpirNT alone (solid and dashed gray lines) are weak under these conditions, but synergize in assembly when combined (blue). SpirNT(A*) synergizes more potently with CapuCT (magenta). (B) Dose dependence of $t_{1/2}$. Solid circles are SpirNT or CapuCT alone (blue and green, respectively; one representative experiment shown for each). Open circles indicate the addition of both proteins. SpirNT, blue; SpirNT(A*), magenta ($n = 3$ independent experiments, each); SpirNT(A*B*C*D*), orange (one representative experiment shown at each concentration). Raw data are shown in Supplemental Figure S1, A–D. (C) Nucleation is stronger on CapuCT/SpirNT(A*)-beads than CapuCT/SpirNT-beads. (D) Quantification of experiments like those shown in C and Figure 5D. Fluorescence around beads is expressed as an average percentage of initial values over time ($n \geq 4$ beads, $n \geq 2$ independent experiments per condition). See *Materials and Methods* for the description of data transformation. Data plotted were obtained using 1-µm-diameter beads, 1 µM actin, and 1 µM profilin, with or without CapuCT (solid or dashed lines, respectively). S, SpirNT-beads; P, profilin; C, CapuCT. SpirNT-bead data are plotted in blue and SpirNT(A*)-bead data in magenta. (E) Rates of fluorescence increase, from D. Mean ± SEM are indicated for each condition. The initial 50 s of images ($t = \sim 30$–80 s) were used to determine rates. A Student's *t* test was performed on each pair of conditions indicated (black brackets). ***, $p < 0.0001$. The difference in activity by SpirNT(A*/WT)-beads (without Capu) was not statistically significant (unequal variance; $p = 0.13$).

WH2 domains are necessary for *Drosophila* oogenesis

The Spir-KIND domain inhibits CapuCT in pyrene-actin assays (Quinlan *et al.*, 2007; Vizcarra *et al.*, 2011). However, genetics indicate that Spir and Capu both play positive roles in oocyte mesh formation (Manseau and Schupbach, 1989; Dahlgaard *et al.*, 2007; Quinlan, 2013). Further, the N-terminal half of Spir (containing only the KIND domain and WH2s) is sufficient to build the mesh (Dahlgaard *et al.*, 2007; Quinlan, 2013). Combined, these data suggest that Spir's WH2 domains contribute to in vivo function. We decided to test this hypothesis directly, in part because Spir(A*)-GFP rescues. In each of Spir's four WH2 domains, we mutated three conserved, hydrophobic residues that contact actin (Figure 1A). These mutations were previously shown to dramatically decrease, if not abolish, actin monomer binding (Quinlan *et al.*, 2005). In vitro, SpirNT with all of these mutations (SpirNT(A*B*C*D*)) does not accelerate actin assembly (Supplemental Figure S1A; Quinlan *et al.*, 2005). nanos-Gal4-vp16–driven expression of Spir(A*B*C*D*)-GFP failed to rescue fertility (hatch rate <2%; Table 1). In oocytes expressing Spir(A*B*C*D*)-GFP, the actin mesh was absent and streaming was premature, consistent with loss of actin assembly activity and loss of fertility (Figure 7, A–C). Thus, we conclude that actin binding by at least one of Spir's WH2 domains is necessary for actin assembly and oogenesis.

Transgene (spir[1]/Df(2L)Exel[6046])[a]	% Hatched[b]	Number counted[b]
Spir-GFP[c]	59	606
Spir(A*B*C*D*)-GFP	<2	431
Spir(A*)-GFP	40	619

[a]Genetic background is in parentheses.
[b]% hatched is reported as the average of at least three independent trials. % hatched is measured 24 h after egg lay. ~95% w^{1118} hatch; 0% spir[1]/Df(2L)Exel[6046] hatch. Number counted is the sum of eggs counted from all trials.
[c]Quinlan (2013).

TABLE 1: Fertility assays.

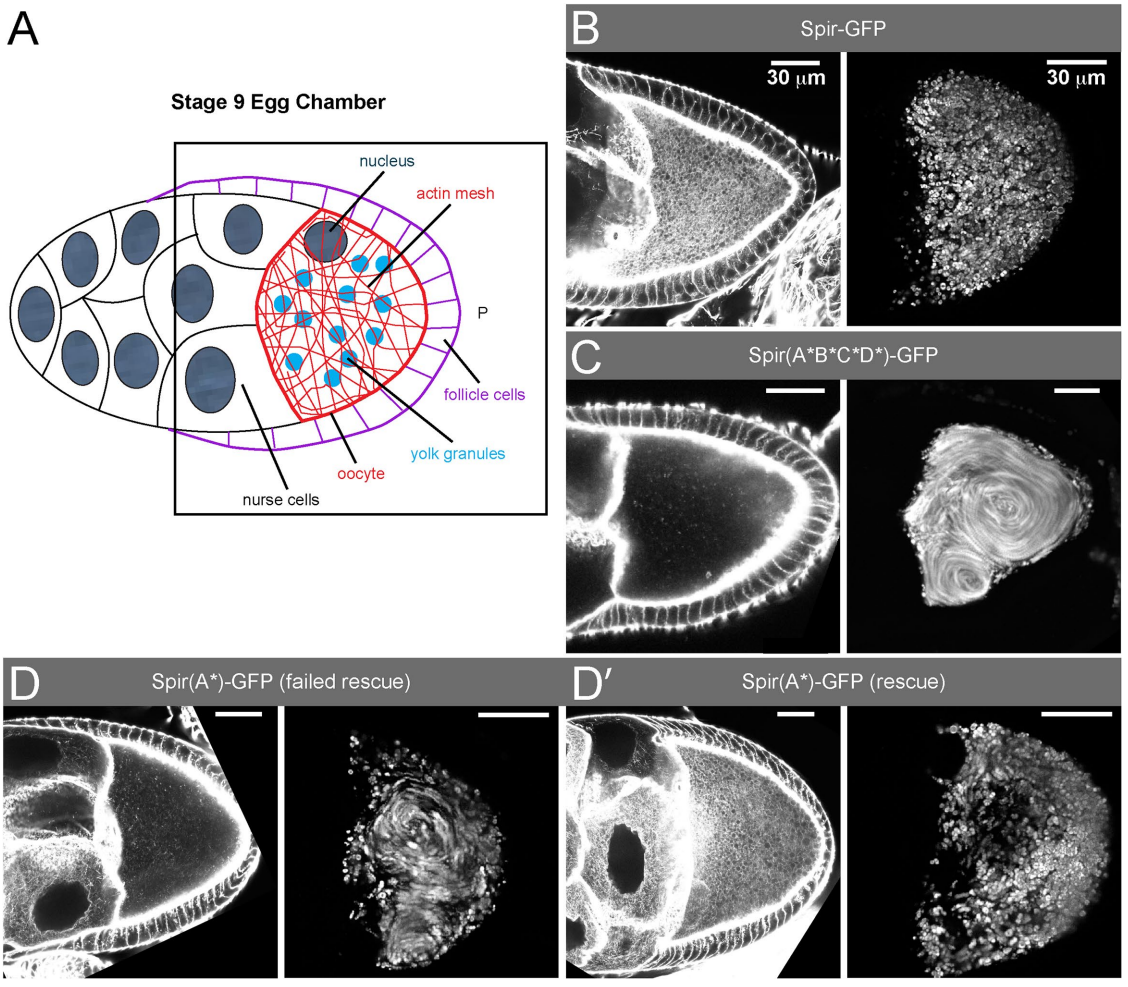

FIGURE 7: WH2 domains are necessary for oogenesis. (A) Cartoon of a stage 9 egg chamber. P, posterior. (B–D) Stage 9 egg chambers dissected from flies with a *spir* null background, expressing Spir-GFP (B), Spir(A*B*C*D*)-GFP (C), or Spir(A*)-GFP (D, D′). Egg chambers were stained with fluorescently labeled phalloidin to detect the presence or absence of mesh (left images) and SD projections of autofluorescent yolk granule positions over 2 min (right images) show the extent of ooplasmic streaming. Expression of Spir(A*)-GFP results in a mixture of failed (D) and successful rescues (11/20 = 55% of stage 9 oocytes had a visible mesh; D′).

DISCUSSION

Spir binds both ends of actin filaments

The bead assay facilitated observation of several steps in actin assembly by Spir and Capu. We found that filaments nucleated on CapuCT/SpirNT-beads grow with their barbed ends away from the bead with enhanced rates, accelerated by CapuCT. Thus, SpirNT and CapuCT separate after nucleation, consistent with genetics results (Quinlan, 2013). We also found that CapuCT-bound barbed ends would subsequently stop growing if they encountered CapuCT/SpirNT-beads, suggesting that the barbed end was passed from CapuCT to SpirNT. To our surprise, we found that SpirNT-beads were sufficient to bind both ends of actin filaments. There are conflicting reports regarding filament-end binding for two classes of tandem-WH2 nucleators: Spir and VopF/L (Liverman *et al.*, 2007; Yu *et al.*, 2011; Pernier *et al.*, 2013, 2016; Burke *et al.*, 2017). The N-termini of WH2 domains bind actin monomers between subdomains 1 and 3 of actin—the surface exposed at the barbed ends of filaments (Hertzog *et al.*, 2004; Chereau *et al.*, 2005). It was, therefore, reasonable to expect tandem-WH2 nucleators to associate with filament barbed ends and surprising when both VopL and Spir were reported to bind filament pointed ends (Quinlan *et al.*, 2005; Namgoong *et al.*, 2011; Yu *et al.*, 2011). Spir nucleates filaments with free barbed ends and inhibits depolymerization of gelsolin-capped filaments, albeit weakly (Quinlan *et al.*, 2005). Spir also caps barbed ends of growing filaments but with nanomolar affinity (Bosch *et al.*, 2007; Montaville *et al.*, 2014). Here we present evidence that these apparently conflicting data are all correct. This is not unprecedented. Namgoong *et al.* (2011) and Burke *et al.* (2017) reported that VopL/F can interact with both ends of actin filaments, depending on the conditions.

Earlier, we did not observe barbed-end binding by Spir when assayed by inhibition of depolymerization (Quinlan *et al.*, 2005). We now report high-affinity barbed-end binding in inhibition of elongation assays. Possibly, Spir binds barbed ends only in the presence of actin monomers as was described for N-Wasp (Co *et al.*, 2007). This contrasts with VopL/F that primarily bind barbed ends of preformed filaments in the absence of free monomer (Burke *et al.*, 2017). The first of Spir's tandem WH2 domains, WH2-A, is necessary to cap barbed ends. It is curious that removing function of this WH2 domain increases the activity of SpirNT. In earlier work, we did not observe a significant difference in actin assembly, with or without WH2-A (Quinlan *et al.*, 2005). The original data were acquired with higher concentrations of both SpirNT and actin, which may have masked the difference. In addition, the data were acquired with a slightly longer construct: 1–520 versus 1–490. One possible explanation for enhanced actin nucleation by SpirNT(A*) is that loss of capping leads to fewer so-called SA_4 complexes (Spir bound to four actin monomers). We and others observed SA_4 complexes when Spir is mixed with actin under polymerizing conditions (Quinlan *et al.*, 2005; Bosch *et al.*, 2007). We originally interpreted these structures as prenuclei. In contrast, Bosch *et al.* (2007) proposed that they are stable structures that sequester actin monomers. Whether there are two paths (i.e., nucleation vs. SA_4 complex), or one (nucleation, with formation of the nucleus from the SA_4 complex being a rate-limiting step), removing capping would likely destabilize the SA_4 structure and could favor nucleation.

How do tandem-WH2-domain nucleators bind filament pointed ends? Single-molecule observations showed that VopL/F remains associated with the pointed ends of filaments it nucleates for ~100 s (Burke *et al.*, 2017). In the absence of actin monomers, VopL/F binds pointed ends for shorter times (~25 s). Higher affinity binding is likely due to the contribution of the VopL/F C-terminal domain, which dimerizes and binds the pointed end. In the case of Spir, weak inhibition of depolymerization may be mediated by a linker or a domain straddling the WH2 domains. Side binding by the C-terminal half of tandem WH2 domains may enhance relatively weak pointed-end binding of both Spir and VopL/F. Side binding by Spir is consistent with the fact that it can sever filaments (Bosch *et al.*, 2007; Chen *et al.*, 2012). The resolution of our bead assay is not sufficient to distinguish between direct binding to the pointed end and binding to the filament side near the pointed end. Additionally, pointed-end elongation is difficult to detect with low actin concentrations and is essentially nonexistent in the presence of profilin. Thus, we speculate that the ability to retain the pointed ends of filaments nucleated by Spir on beads reflects enhanced binding, perhaps to both filament sides and the pointed end, due to clustering on beads (Figure 8A). Multiple cases of emergent behavior of clustered WH2 domains have been reported. Spir nucleates more potently when clustered on gold particles (Ito *et al.*, 2011). VopL retains the pointed end of ~10% of nucleated filaments for several minutes (compared with seconds for ~80% of filaments) and accelerates barbed-end elongation of ~8% of filaments when clustered on Qdots (Namgoong *et al.*, 2011); and Ena/VASP are potent elongation factors when clustered on beads (Breitsprecher *et al.*, 2008; Winkelman *et al.*, 2014). In sum, WH2 domains can associate with both ends of actin filaments and they are likely to function as part of a larger context that dictates their activity (Dominguez, 2016).

How do Spir and Capu synergize?

Synergy of actin assembly can be explained by enhanced nucleation and/or elongation. In the cases of Bud6/Bni1 and APC/mDia1, nucleation is enhanced (Graziano *et al.*, 2011; Breitsprecher *et al.*, 2012). We propose that increased nucleation is also the dominant source of synergy for Spir/Capu. The ping-pong model suggests that Spir and Capu (Fmn2) enhance elongation by dynamic exchange at the barbed ends of filaments. A key element of the ping-pong model is that Fmn2 binds barbed ends with a slow on-rate. Thus, by recruiting Fmn2 to barbed ends, Spir increases the fraction of time that elongation is enhanced by the formin. We found that synergistic assembly of profilin–actin is actually improved in the absence of Spir binding to barbed ends (CapuCT+SpirNT(A*)). We also directly observed increased nucleation in bead assays: CapuCT/SpirNT-beads nucleate 6× and 10× more potently than SpirNT-beads, with or without a functional WH2-A, respectively (Figures 5D and 6, C–E). A full comparison (i.e., nucleation by SpirNT-beads and CapuCT-beads, vs. CapuCT/SpirNT-beads) was precluded by the inactivity of CapuCT-beads, regardless of the coupling method. Finally, we see a fourfold increase in nucleation by CapuCT/SpirNT(A*)-beads compared with wild-type CapuCT/SpirNT-beads, similar to the approximately three times decrease in $t_{1/2}$ in bulk pyrene assays (Figure 6B). Thus, we conclude that nucleation is the major source of enhanced actin assembly mediated by Spir/Capu synergy.

Ping-ponging may still take place and contribute to mesh assembly. We observe transfer of Capu-bound barbed ends to Spir (Figure 4C and Supplemental Video 8), consistent with one half of ping-pong. We do not see transfer in the other direction, but our bead-based assay is not well suited to studying this process, as we do not have excess Spir or Capu in solution. (The original observation of ping-pong was made with all proteins in solution [Montaville *et al.*, 2014].) Importantly, the intermediate phenotype we observe in flies expressing Spir(A*)-GFP (Figure 7, D and D′, and Table 1) could

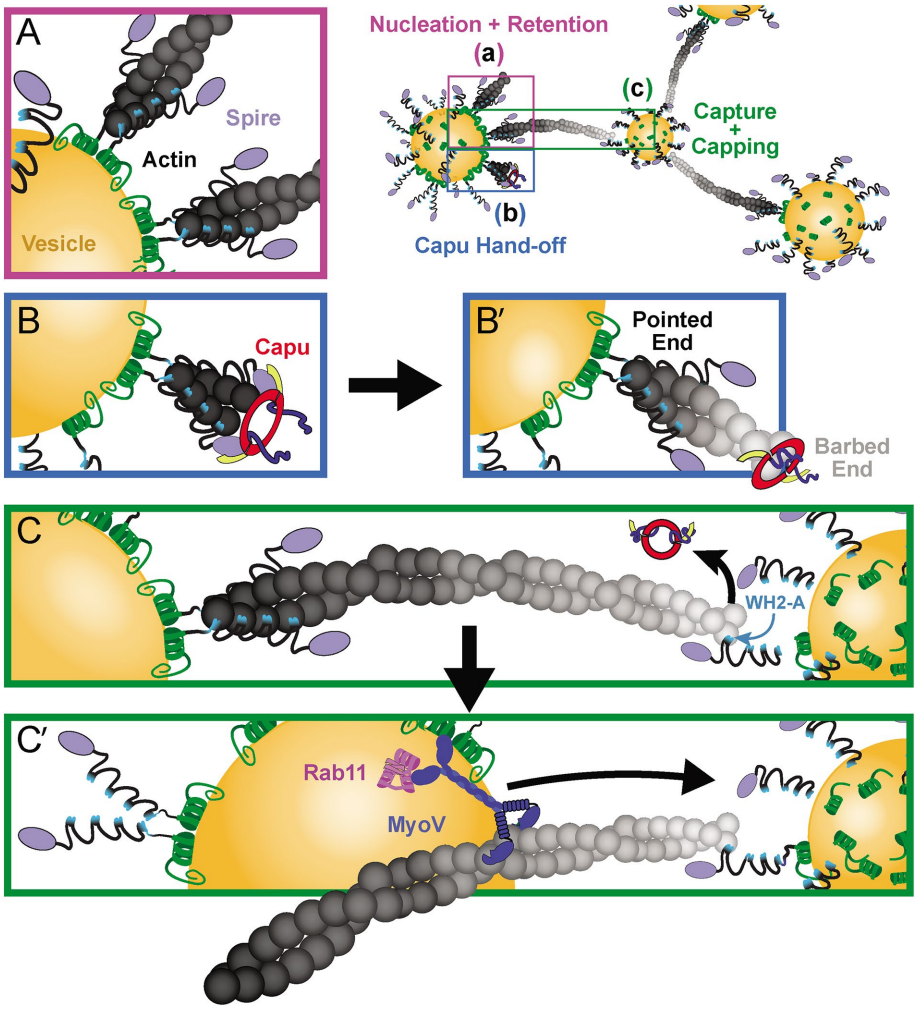

FIGURE 8: Model of Spir–Capu synergy. (A) Spir is directed to vesicles through its phospholipid-binding mFYVE domain (green helix). The clustering of Spir on vesicles may enhance its affinity for filament pointed ends. Each of Spir's tandem, WH2 domains (light blue) can bind to an actin subunit (dark-gray spheres). (B) Spir and Capu interact through their respective KIND (purple) and tail (yellow) domains. (B′) Spir retains a filament's pointed end (dark gray), while Capu separates from Spir to elongate its barbed end (light gray). (C) A filament's barbed end is captured and capped by Spir's WH2-A domain (light blue), displacing Capu. Spir's bipolar filament binding may tether vesicles, as shown. (C′) Associated with Rab11 (pink) and Spir on vesicles, MyoV (dark blue) may tow a nucleating vesicle (left) toward another, receiving (filament capturing) vesicle (right).

indicate that, while not necessary, ping-ponging may enhance mesh assembly in the oocyte. Perhaps Spir helps Capu fall off of filaments when they reach their target. Additionally, Spir could pass the filament to another protein that anchors it at the vesicle even more stably, influencing the dynamics of the mesh. It is also possible that capping serves an important role in vivo, independent of the processes we are studying here.

The classical nucleation promoting factors (NPFs), N-Wasp and Scar, bind actin monomers and the Arp2/3 complex to stimulate nucleation by the Arp2/3 complex (Machesky *et al.*, 1999; Welch and Mullins, 2002). Similarly, the yeast NPF, Bud6, binds an actin monomer and the formin Bni1 to stimulate nucleation by Bni1 (Graziano *et al.*, 2011; Tu *et al.*, 2012; Park *et al.*, 2015). In each of these cases, the NPF has negligible independent activity. In contrast, APC and Spir can nucleate alone, as well as synergize with a formin (Quinlan *et al.*, 2005; Moseley *et al.*, 2007; Okada *et al.*, 2010; Montaville *et al.*, 2014). We note that Spir's nucleation activity in the presence of profilin correlates with synergy: in the absence of nucleation by SpirNT(A*B*C*D*), no synergy is observed; when nucleation is augmented (SpirNT(A*) nucleation is approximately three times stronger than SpirNT), synergy with Capu is also enhanced over wild type (approximately four times). These are only two data points, but they suggest that Spir's nucleation contributes to synergy, as opposed to Spir acting as a passive actin-binding protein, or NPF. In fact, if monomer delivery were Spir's main role, one might expect SpirNT(A*) to be a weaker Capu activator because it has fewer functional WH2 domains. Thus, we propose that Spir and Capu collaborate by a mechanism similar to that of APC/mDia1; Spir nucleates seeds that are elongated by Capu (Figure 8B).

In vivo implications

The filament orientation we observe (barbed ends away from the bead) reflects the fact that Spir is attached to the beads and Capu is bound to Spir in our assays. As we and others have shown, when a formin is bound to a bead, filaments grow with their barbed ends at the bead surface. Both mSpire and Fmn-2 are enriched on Rab-11 vesicles. We speculate that Fmn2 is affiliated by binding mSpire as opposed to an independent association with the vesicle. We base this on the finding that mSpire binds directly to membranes and the fact that, in flies, GFP-Capu is diffuse throughout the oocyte (Quinlan, 2013; Tittel *et al.*, 2015). If we are correct, then the geometry in our assays mimics the in vivo geometry and indicates that the actin filaments are oriented opposite to what was originally proposed by others (Schuh, 2011; Montaville *et al.*, 2014). Long distance transport is still possible with this orientation of filaments (Figure 8C). Instead of myosin V capturing filaments from a neighboring vesicle, Spir or another protein could capture a growing filament, and myosin V, on the vesicle from which the filament originated, could walk along the filament pulling the vesicle toward its neighbor (Figure 8C′). In this case, pointed-end attachment would not have to be as long lasting as barbed-end capture. These conditions are surprisingly well satisfied in our simplified system.

Increased Capu expression is sufficient to build a mesh in the absence of Spir or in the absence of direct interaction with Spir (Dahlgaard *et al.*, 2007; Quinlan, 2013). In these cases, the mesh is not as dense or as long lived. No mesh is built when exogenous Spir expression is driven in the absence of Capu (Dahlgaard *et al.*, 2007). Thus, we propose that Spir's primary role in vivo is as an NPF, enhancing Capu's actin assembly activity. NPFs offer an additional level of control in the cell and may relieve the nucleation-dampening effect of profilin on formins like Capu. In the case of the fly oocyte, we also note that the cytoplasm is enriched with

microtubules that potently inhibit Capu by binding to its tail, where the Spir-KIND domain also binds (Roth-Johnson *et al.*, 2014). Thus, Spir is well suited to simultaneously protect Capu from inhibitory factors and amplify its activity. The fact that Spir(A*)-GFP expression largely rescues loss of Spir indicates that barbed-end binding by Spir is not necessary for oogenesis. We note, however, that actin nucleation by SpirNT(A*) alone and with Capu is enhanced, which could compensate for loss of ping-ponging or other barbed-end binding roles of Spir.

MATERIALS AND METHODS

DNA constructs

CapuCT (aa 467–1059) constructs were expressed from a modified pET15b vector with an N-terminal hexahistidine tag (Vizcarra *et al.*, 2011). All other proteins were expressed from a modified pET20b(+) vector with no affinity tag. A native polyhistidine region within the Spir-KIND domain is sufficient for binding of these constructs to TALON resin (Clontech).

Gibson cloning was employed for the scar-free introduction of Avidity's 45 base pair Avitag (translated sequence: GLNDIFEAQKIEWHE) to all proteins requiring biotinylation for bead conjugation. This tag was introduced to the C-terminus of all constructs.

Expression, purification, and biotinylation of proteins

Actin was purified from *Acanthamoeba castellani* as described (Zuchero, 2007) and stored in G-buffer (2 mM Tris-Cl, pH 8.0, 0.1 mM $CaCl_2$, 0.2 mM ATP, 0.5 mM Tris(2-carboxyethyl)phosphine [TCEP], 0.04% sodium azide).

Expression was induced in Rosetta (DE3) cells (EMD Biosciences). Bacteria were grown in Terrific Broth medium supplemented with 100 mg/l ampicillin and 32 mg/l chloramphenicol. Cells were grown to an optical density of 0.6 at 37°C, cooled to 18°C for 1 h, induced with 250 µM isopropyl β-D-1-thiogalactopyranoside (IPTG), and shaken for 18 h at 18°C. Bacteria were harvested by centrifugation. Pellets were washed once with ice-cold phosphate-buffered saline (PBS), flash-frozen in liquid nitrogen, and stored at –80°C.

All purification steps were carried out at 4°C or on ice. Thawed cells were diluted at least twofold with lysis buffer (50 mM sodium phosphate, pH 8.0, 1 mM β-ME, 300 mM NaCl) supplemented with 1 mM phenylmethylsulfonyl fluoride and 2 µg/ml DNaseI, and then lysed by microfluidizing, two to three times. Cell debris was removed by centrifugation at 20,000 × *g* for 20 min at 4°C. Clarified lysates were then rocked with TALON resin for 1 h at 4°C (4 ml slurry for every 1 l culture pellet). The TALON resin was washed with 20 column volumes of lysis buffer, followed by washing with 20 column volumes of wash buffer (lysis buffer, at pH 7.0). Proteins were eluted with elution buffer (wash buffer, plus 200 mM imidazole), until little or no protein remained on the column, as determined by a Coomassie-stained dot-blot of the eluates.

TALON eluates were pooled and dialyzed twice for 2 h and once overnight against 1 l volumes of 10 mM Tris, 1 mM dithiothreitol (DTT), pH 8.0; or 5 ml of the most concentrated eluates was buffer exchanged into the same, using a PD-10 desalting column (GE Life Sciences). Protein was loaded onto a MonoQ anion exchange column (GE Life Sciences) and eluted using a gradient of 50–500 mM KCl over 60 column volumes for Spir-KIND, 50–250 mM KCl over 100 column volumes for CapuCT, or 0–500 mM KCl over 60 column volumes for SpirNT. Pooled fractions from the MonoQ column were again dialyzed or buffer exchanged as described above. Unless tagged with an Avitag, 50% glycerol was added to the overnight dialysis step (1:1 glycerol:buffer). The protein was flash-frozen in liquid nitrogen in 10–50 µl aliquots and stored at –80°C.

If tagged with an Avitag, 2 ml of the protein was added to 223 µl Biomix B and 5 µl (5 µg) BirA (both from Avidity) and rocked overnight at 4°C. The reaction was again loaded onto a MonoQ anion exchange column and eluted as described above. Pooled fractions from the MonoQ column were dialyzed or buffer exchanged as described above, with 50% glycerol added to the overnight dialysis step and flash-frozen in liquid nitrogen.

Spir-KIND, SpirNT, and CapuCT concentrations were calculated based on their absorbances at 280 nm (ε_{280} = 17,452 cm^{-1} M^{-1} for KIND, 25,575 cm^{-1} M^{-1} for Spir-NT, and 75,200 cm^{-1} M^{-1} for CapuCT; Quinlan *et al.*, 2007).

Purified, SNAP-tagged mDia1 protein was generously provided by the Kovar lab (University of Chicago).

Pyrene-actin assembly assays

Bulk actin assembly assays were carried out essentially as described (Zuchero, 2007). Briefly, actin (5% pyrene labeled) was incubated for 2 min at 25°C with 200 µM ethylene glycol-bis(β-aminoethyl ether)-*N*,*N*,*N*′,*N*′-tetraacetic acid (EGTA) and 50 µM $MgCl_2$ to convert Ca-actin to Mg-actin. When included in the experiment, *Schizosaccharomyces pombe* profilin (typically 2:1 profilin:actin) was incubated with actin for 2 min at 25°C before conversion to Mg-actin. Polymerization was initiated by adding polymerization buffer ("KMEH," final concentration: 10 mM HEPES, pH 7.0, 1 mM EGTA, 50 mM KCl, 1 mM $MgCl_2$) to the Mg-actin. Additional components, such as CapuCT, SpirNT, and capping protein, were combined in the polymerization buffer before addition to Mg-actin. Fluorescence was monitored in a TECAN F200 with $\lambda_{ex} = 360 \pm 17$ nm and $\lambda_{em} = 400 \pm 10$ nm.

Actin seeds were prepared by polymerizing 5 µM actin at 25°C for 1 h in KMEH. The filaments were dispensed in 5 µl aliquots and allowed to reequilibrate for 2–3 h at 25°C. SpirNT was incubated with filaments for 3 min at 25°C. During this incubation time, monomeric actin was converted to Mg-actin. Using a cut pipette tip to prevent shearing, polymerization buffer was added to Mg-actin and then mixed with seeds plus SpirNT. The slope of the pyrene fluorescence trace between 200 and 500 s was considered the elongation rate.

SpirNT-bead preparation

Streptavidin-coated microspheres were either colorless or Flash Red fluorescent, with mean diameters of ~100 nm or ~1 µm (Bangs Laboratories), respectively. Spheres were washed twice with ~20 volumes of KMEH, resuspended in 1 volume of KMEH + 1 mg/ml bovine serum albumin, and added in 10 µl aliquots to 40 µl protein mixtures in KMEH. The protein mixture always included a saturating concentration of SpirNT-biotin (400 nM). When included, 200 nM (dimeric) CapuCT was preincubated with the SpirNT-biotin on ice for 10 min to allow the formation of SpirNT–CapuCT complexes. Protein mixtures were incubated with spheres for 10 min on ice and then spun for 10 min at 10,000× rpm and 4°C. Buffer and excess proteins (i.e., unbound SpirNT–biotin and CapuCT) were aspirated and pellets were gently resuspended in 30 µl KMEH. Pellets were briefly sonicated (~5 s) if clumped and not well dispersed when visualized by TIRF microscopy.

TIRF microscopy assays

Coverslips were prepared and functionalized with polyethylene glycol (final surface composition, 97% methoxy-PEG and 3% biotin-PEG; JenKem Technology, Allen, TX) as previously described (Bor *et al.*, 2012). Biotinylated coverslips were stored in a sealed

container at 4°C for up to 2 mo before use. Flow cells with volumes of ~10–15 µl were assembled using thin strips of double-stick tape.

All buffers were flowed into cells in 25 µl volumes in the following order: 1) blocking buffer (1X PBS, pH 8.0, 1% pluronic, 0.1 mg/ml casein) with 2 min incubation; 2) TIRF buffer (50 mM KCl, 1 mM $MgCl_2$, 1 mM EGTA, 10 mM HEPES, pH 7.0, 0.2 mM ATP, 50 mM DTT, 0.2% methylcellulose, 20 mM glucose); 3) prepared beads (5 µl resuspended beads, 25 µl TIRF buffer) with 2 min incubation; 4) TIRF buffer; 5) TIRF buffer, supplemented with GCC mix (0.25 mg/ml glucose oxidase, 0.05 mg/ml catalase, 0.8 mg/ml casein), actin (typically 1 µM, 20% Oregon Green labeled), and profilin and/or capping protein, when appropriate. In this final step, actin and profilin (when present) were mixed and incubated for 1 min, then added to the other buffer components immediately before being flowed into the cell.

Time zero was defined as the moment the final 25 µl mix, including actin, was entirely added. Polymerization was visualized immediately (typically, t = ~30 s) on a DMI6000B TIRF microscope (Leica, Wetzlar, Germany), controlled by LAS X (Leica software). Images were acquired with a DU897 EMCCD camera (Andor) and 100×/1.47 HCX PL APO objective (Leica) at ~25°C. All analyses were performed on raw data in FIJI. The brightness and contrast of figure images were minimally adjusted for clarity of image features. Filament lengths, elongation rates, and kymographs were analyzed/prepared with JFilament incorporated in FIJI (Smith *et al.*, 2010). Plots were made and statistical analyses conducted in Kaleidagraph. Filament dwell times were obtained by manually tracking individual, retained filaments until clearly released from a bead. Some filaments did not become clearly visible in the TIRF plane until some growth had already occurred. In these cases, time was added to the measured retention period, proportional to the initial length of the filament and the average filament elongation rate observed in the experiment.

For two-color experiments, 1 µM Cy3B-labeled actin was introduced to the functionalized, bead-bound flow cell. Following this (step 5 of the aforementioned protocol), and after allowing beads to briefly (1–2 mins) polymerize the Cy3B-actin, the following components were flowed in: 6) TIRF buffer supplemented with 1 µM phalloidin, with 2 min incubation; 7) TIRF buffer supplemented with GCC mix, 600 nM 20% labeled OG-actin, and 300 nM profilin. Polymerization was visualized as described above.

For the plots generated in Figure 6, D and E, circles of 10 and 11 pixel (px) radii (1.6 and 1.76 µm, respectively) were drawn around the centroids of each bead. Actin fluorescence was measured within these circles over time. The integrated density measurements of the 10 px circles were subtracted from those of their concentric, 11 px circles, to measure 1-px-wide (160 nm) bands of actin fluorescence, 1.6 µm away from beads. A script that performs these operations in FIJI is available upon request.

Fluorescence measurements in Figure 6, D and E, are expressed as a fraction of their initial values (i.e., a 10% increase = 1.1). Discrepancies in initial fluorescence values for different bead types were observed, in part, due to real differences in assembly rates, because actin polymerization could not be observed instantly. To scale these differences in assembly before image collection, the average starting values of each bead type were compared. The larger ratio of these two values was used as a multiplier for the more active bead type. For example, if measurements of SpirNT(A*)- and SpirNT-beads were 110% their initial values, these quantities would each be plotted as "1.1." However, if the average, initial values of SpirNT(A*)-beads were twice those of SpirNT-beads, the quantities would be plotted as "2.2" and "1.1," respectively, reflecting the twofold greater assembly by SpirNT(A*)-beads before image collection.

Drosophila stocks

The following stocks were obtained from the Bloomington Drosophila Stock Center: *spir*[1] and *capu*[1] (Manseau and Schüpbach, 1989); Df(2L)Exel[6046] (Exelixis); and nos-GAL4-vp16 (Van Doren *et al.*, 1998). Mutant SpirB-GFP transgenes were generated by inserting the coding region of spir (CG10076-RB) with point mutations created by QuikChange mutagenesis, between the *Kpn*I and *Spe*I sites of pTIGER (Ferguson *et al.*, 2012) with mEGFP inserted between the *Bam*HI and *Xba*I sites. pTIGER plasmids were integrated at the attP2 landing site by BestGene.

Fertility assays

Approximately 100 test females were crossed to 40 wild-type males and kept on apple plates for two nights at 25°C. Flies were precleared on a fresh plate with yeast paste for at least 1.5 h; the plate was changed and eggs laid over the next 3 h were collected. Typically, 100 eggs were laid in this time period. Eggs were transferred to a fresh plate and stored at 25°C. The number of eggs that hatched after 24 h was recorded. Each trial was repeated at least three times with independent crosses.

Fly oocyte microscopy and staining

The visualization of cytoplasmic flows and the actin mesh were performed on a Leica SPE I inverted confocal microscope. Flies were kept at 25°C and fed yeast paste for ~24 h before an experiment. Flows were visualized by imaging autofluorescent yolk granules of egg chambers teased apart in Halocarbon oil 700. The actin mesh was stained as described by Dahlgaard *et al.* (2007) with modifications. Briefly, ovaries were dissected, teased apart, and fixed in 10% paraformaldehyde/PBS (pH 7.4) for a total of less than 20 min. Samples were stained with 1 µM Alexa Fluor 488–phalloidin diluted in 0.3% Triton X-100/PBS for 25 min at room temperature. Samples were then washed extensively and mounted in ProLong Gold with 4′,6-diamidino-2-phenylindole (DAPI). Images were recorded within 24 h of staining because phalloidin staining quality degraded over time, as has been reported (Dahlgaard *et al.*, 2007).

ACKNOWLEDGMENTS

We acknowledge all members of the Quinlan lab for their tireless support and thank David Kovar for generously gifting us purified, SNAP-tagged mDia1. This work was supported by the UCLA Cellular and Molecular Biology Training Program, T32 GM007185 (A.O.B.), March of Dimes Grant no. 1-FY15-290 (M.E.Q.), and National Institutes of Health (NIH) Grant no. R01 GM-096133 (M.E.Q.). Stocks obtained from the Bloomington Drosophila Stock Center (NIH P40OD018537) were used in this study.

REFERENCES

Ahmed WW, Fodor É, Almonacid M, Bussonnier M, Verlhac M-H, Gov N, Visco P, van Wijland F, Betz T (2018). Active mechanics reveal molecular-scale force kinetics in living oocytes. Biophys J 114, 1667–1679.

Almonacid M, Ahmed WW, Bussonnier M, Mailly P, Betz T, Voituriez R, Gov NS, Verlhac M-H (2015). Active diffusion positions the nucleus in mouse oocytes. Nat Cell Biol 17, 470–479.

Azoury J, Lee KW, Georget V, Rassinier P, Leader B, Verlhac M-H (2008). Spindle positioning in mouse oocytes relies on a dynamic meshwork of actin filaments. Curr Biol 18, 1514–1519.

Bor B, Vizcarra CL, Phillips ML, Quinlan ME (2012). Autoinhibition of the formin Cappuccino in the absence of canonical autoinhibitory domains. Mol Biol Cell 23, 3801–3813.

Bosch M, Le KHD, Bugyi B, Correia JJ, Renault L, Carlier M-F (2007). Analysis of the function of spire in actin assembly and its synergy with formin and profilin. Mol Cell 28, 555–568.

Breitsprecher D, Jaiswal R, Bombardier JP, Gould CJ, Gelles J, Goode BL (2012). Rocket launcher mechanism of collaborative actin assembly defined by single-molecule imaging. Science 336, 1164–1168.
Breitsprecher D, Kiesewetter AK, Linkner J, Urbanke C, Resch GP, Small JV, Faix J (2008). Clustering of VASP actively drives processive, WH2 domain-mediated actin filament elongation. EMBO J 27, 2943–2954.
Burke TA, Harker AJ, Dominguez R, Kovar DR (2017). The bacterial virulence factors VopL and VopF nucleate actin from the pointed end. J Cell Biol 216, 1267–1276.
Chen CK, Sawaya MR, Phillips ML, Reisler E, Quinlan ME (2012). Multiple forms of Spire-actin complexes and their functional consequences. J Biol Chem 287, 10684–10692.
Chereau D, Kerff F, Graceffa P, Grabarek Z, Langsetmo K, Dominguez R (2005). Actin-bound structures of Wiskott–Aldrich syndrome protein (WASP)-homology domain 2 and the implications for filament assembly. Proc Natl Acad Sci USA 102, 16644–16649.
Co C, Wong DT, Gierke S, Chang V, Taunton J (2007). Mechanism of actin network attachment to moving membranes: barbed end capture by N-WASP WH2 domains. Cell 128, 901–913.
Dahlgaard K, Raposo AA, Niccoli T, St Johnston D (2007). Capu and Spire assemble a cytoplasmic actin mesh that maintains microtubule organization in the *Drosophila* oocyte. Dev Cell 13, 539–553.
Dominguez R (2016). The WH2 domain and actin nucleation: necessary but insufficient. Trends Biochem Sci 41, 478–490.
Ferguson SB, Blundon MA, Klovstad MS, Schüpbach T (2012). Modulation of gurken translation by insulin and TOR signaling in *Drosophila*. J Cell Sci 125, 1407–1419.
Graziano BR, DuPage AG, Michelot A, Breitsprecher D, Moseley JB, Sagot I, Blanchoin L, Goode BL (2011). Mechanism and cellular function of Bud6 as an actin nucleation–promoting factor. Mol Biol Cell 22, 4016–4028.
Hertzog M, van Heijenoort C, Didry D, Gaudier M, Coutant J, Gigant B, Didelot G, Preat T, Knossow M, Guittet E, *et al*. (2004). The β-thymosin/WH2 domain: structural basis for the switch from inhibition to promotion of actin assembly. Cell 117, 611–623.
Holubcová Z, Howard G, Schuh M (2013). Vesicles modulate an actin network for asymmetric spindle positioning. Nat Cell Biol 15, 937–947.
Ito T, Narita A, Hirayama T, Taki M, Iyoshi S, Yamamoto Y, Maéda Y, Oda T (2011). Human spire interacts with the barbed end of the actin filament. J Mol Biol 408, 18–25.
Kovar DR, Pollard TD (2004). Insertional assembly of actin filament barbed ends in association with formins produces piconewton forces. Proc Natl Acad Sci USA 101, 14725–14730.
Leader B, Lim H, Carabatsos MJ, Harrington A, Ecsedy J, Pellman D, Maas R, Leder P (2002). Formin-2, polyploidy, hypofertility and positioning of the meiotic spindle in mouse oocytes. Nat Cell Biol 4, 921–928.
Liverman AD, Cheng HC, Trosky JE, Leung DW, Yarbrough ML, Burdette DL, Rosen MK, Orth K (2007). Arp2/3-independent assembly of actin by Vibrio type III effector VopL. Proc Natl Acad Sci USA 104, 17117–17122.
Machesky LM, Mullins RD, Higgs HN, Kaiser DA, Blanchoin L, May RC, Hall ME, Pollard TD (1999). Scar, a WASp-related protein, activates nucleation of actin filaments by the Arp2/3 complex. Proc Natl Acad Sci USA 96, 3739–3744.
Manseau LJ, Schupbach T (1989). Cappuccino and spire: two unique maternal-effect loci required for both the anteroposterior and dorsoventral patterns of the *Drosophila* embryo. Genes Dev 3, 1437–1452.
Montaville P, Jégou A, Pernier J, Compper C, Guichard B, Mogessie B, Schuh M, Romet-Lemonne G, Carlier M-F (2014). Spire and formin 2 synergize and antagonize in regulating actin assembly in meiosis by a ping-pong mechanism. PLoS Biol 12, e1001795.
Moseley JB, Bartolini F, Okada K, Wen Y, Gundersen GG, Goode BL (2007). Regulated binding of adenomatous polyposis coli protein to actin. J Biol Chem 282, 12661–12668.
Namgoong S, Boczkowska M, Glista MJ, Winkelman JD, Rebowski G, Kovar DR, Dominguez R (2011). Mechanism of actin filament nucleation by *Vibrio* VopL and implications for tandem W domain nucleation. Nat Struct Mol Biol 18, 1060–1067.
Okada K, Bartolini F, Deaconescu AM, Moseley JB, Dogic Z, Grigorieff N, Gundersen GG, Goode BL (2010). Adenomatous polyposis coli protein nucleates actin assembly and synergizes with the formin mDia1. J Cell Biol 189, 1087–1096.
Park E, Graziano BR, Zheng W, Garabedian M, Goode BL, Eck MJ (2015). Structure of a Bud6/actin complex reveals a novel WH2-like actin monomer recruitment motif. Structure 23, 1492–1499.
Pechlivanis M, Samol A, Kerkhoff E (2009). Identification of a short Spir interaction sequence at the C-terminal end of formin subgroup proteins. J Biol Chem 284, 25324–25333.
Pernier J, Orban J, Avvaru BS, Jégou A, Romet-Lemonne G, Guichard B, Carlier M-F (2013). Dimeric WH2 domains in Vibrio VopF promote actin filament barbed-end uncapping and assisted elongation. Nat Struct Mol Biol 20, 1069–1076.
Pernier J, Shekhar S, Jegou A, Guichard B, Carlier M-F (2016). Profilin interaction with actin filament barbed end controls dynamic instability, capping, branching, and motility. Dev Cell 36, 201–214.
Pfender S, Kuznetsov V, Pleiser S, Kerkhoff E, Schuh M (2011). Spire-type actin nucleators cooperate with formin-2 to drive asymmetric oocyte division. Curr Biol 21, 955–960.
Quinlan ME (2013). Direct interaction between two actin nucleators is required in *Drosophila* oogenesis. Development 140, 4417–4425.
Quinlan ME, Heuser JE, Kerkhoff E, Mullins RD (2005). *Drosophila* Spire is an actin nucleation factor. Nature 433, 382–388.
Quinlan ME, Hilgert S, Bedrossian A, Mullins RD, Kerkhoff E (2007). Regulatory interactions between two actin nucleators, Spire and Cappuccino. J Cell Biol 179, 117–128.
Rasson AS, Bois JS, Pham DSL, Yoo H, Quinlan ME (2015). Filament assembly by Spire: key residues and concerted actin binding. J Mol Biol 427, 824–839.
Roth-Johnson EA, Vizcarra CL, Bois JS, Quinlan ME (2014). Interaction between microtubules and the *Drosophila* formin Cappuccino and its effect on actin assembly. J Biol Chem 289, 4395–4404.
Schuh M (2011). An actin-dependent mechanism for long-range vesicle transport. Nat Cell Biol 13, ncb2353.
Schuh M, Ellenberg J (2008). A new model for asymmetric spindle positioning in mouse oocytes. Curr Biol 18, 1986–1992.
Smith MB, Li H, Shen T, Huang X, Yusuf E, Vavylonis D (2010). Segmentation and tracking of cytoskeletal filaments using open active contours. Cytoskeleton 67, 693–705.
Tittel J, Welz T, Czogalla A, Dietrich S, Samol-Wolf A, Schulte M, Schwille P, Weidemann T, Kerkhoff E (2015). Membrane targeting of the Spir·Formin actin nucleator complex requires a sequential handshake of polar interactions. J Biol Chem 290, 6428–6444.
Tu D, Graziano BR, Park E, Zheng W, Li Y, Goode BL, Eck MJ (2012). Structure of the formin-interaction domain of the actin nucleation-promoting factor Bud6. Proc Natl Acad Sci USA 109, E3424–E3433.
Van Doren M, Williamson AL, Lehmann R (1998). Regulation of zygotic gene expression in *Drosophila* primordial germ cells. Curr Biol 8, 243–246.
Vizcarra CL, Kreutz B, Rodal AA, Toms AV, Lu J, Zheng W, Quinlan ME, Eck MJ (2011). Structure and function of the interacting domains of Spire and Fmn-family formins. Proc Natl Acad Sci USA 108, 11884–11889.
Welch MD, Mullins RD (2002). Cellular control of actin nucleation. Annu Rev Cell Dev Biol 18, 247–288.
Winkelman JD, Bilancia CG, Peifer M, Kovar DR (2014). Ena/VASP enabled is a highly processive actin polymerase tailored to self-assemble parallel-bundled F-actin networks with Fascin. Proc Natl Acad Sci USA 111, 4121–4126.
Yu B, Cheng HC, Brautigam CA, Tomchick DR, Rosen MK (2011). Mechanism of actin filament nucleation by the bacterial effector VopL. Nat Struct Mol Biol 18, 1068–1074.
Zeth K, Pechlivanis M, Samol A, Pleiser S, Vonrhein C, Kerkhoff E (2011). Molecular basis of actin nucleation factor cooperativity: crystal structure of the Spir-1 kinase non-catalytic C-lobe domain (KIND)•formin-2 formin SPIR interaction motif (FSI) complex. J Biol Chem 286, 30732–30739.
Zuchero JB (2007). In vitro actin assembly assays and purification from *Acanthamoeba*. Methods Mol Biol 370, 213–226.